NASA TN D-687

TECHNICAL NOTE

D-687

EXPERIMENTAL AND THEORETICAL STUDY OF HEAT CONDUCTION FOR AIR UP TO 5000° K

By Tzy-Cheng Peng and Warren F. Ahtye

Ames Research Center
Moffett Field, Calif.

NATIONAL AERONAUTICS AND SPACE ADMINISTRATION

WASHINGTON

February 1961

NATIONAL AERONAUTICS AND SPACE ADMINISTRATION

TECHNICAL NOTE D-687

EXPERIMENTAL AND THEORETICAL STUDY OF HEAT CONDUCTION FOR AIR UP TO 5000° K

By Tzy-Cheng Peng and Warren F. Ahtye

SUMMARY

The theoretical value of the integral of thermal conductivity is compared with the experimental values from shock-tube measurements. The particular case considered is the one-dimensional nonsteady flow of heat through air at constant pressure. This approach has been previously described in NASA TR R-27. However, the correlation between theory and experiment was uncertain because of the large scatter in the experimental data. In this paper, an attempt is made to improve the correlation by use of a more refined calculation of the integral of thermal conductivity, and by use of improved experimental techniques and instrumentation. As a result of these changes, a much closer correlation is shown between the experimental and theoretical heat-flux potentials. This indicates that the predicted values of the coefficient of thermal conductivity for high-temperature air may be suitably accurate for many engineering needs, up to the limits of the test (4600° K).

INTRODUCTION

Under normal conditions of temperature and pressure, the variation of the thermal conductivity with temperature for most gases is similar to that for the ideal gas, where the thermal conductivity is approximately proportional to the square root of the temperature. For these conditions, the only excited degrees of freedom are translational and rotational. However, the thermal conductivity deviates from the ideal-gas variation as the temperature increases to a point where the inactive degrees of freedom are excited and where chemical reactions are initiated (ref. 1). The chemical reactions cause the thermal conductivity to become pressure-dependent as well. The mechanism of thermal conduction in a gas medium with a temperature gradient can be explained as a transport of thermal energy. The excitation and chemical reactions enable the molecules to absorb thermal energy in high-temperature regions and to release the energy in low-temperature regions.

In the case of air, the previously inactive modes which are excited are vibration of the molecules and transition of electrons to higher energy states. The important chemical reactions are the formation of nitric oxide, the dissociation of oxygen, the dissociation of nitrogen,

and finally, if a sufficiently high temperature is reached, the ionization of oxygen and nitrogen. Since each of these phases reaches its maximum at a different region of pressure and temperature, the variation of thermal conductivity is quite complex.

Hansen (ref. 2) made calculations of coefficients of thermal conductivity which included the aforementioned effects, with the exception of the formation of nitric oxide. In reference 3, the single effect of oxygen dissociation on the thermal conductivity of air was evaluated from measurements in a shock tube. The purposes of that experiment were to evaluate an average coefficient of thermal conductivity, and to check the theoretical calculations. The experimental results generally agreed with the theoretical estimates, though there was a rather large amount of scatter in the data.

The purposes of this paper are: (1) to present a supplementary set of data which were obtained with improved experimental instrumentation and techniques; and (2) to present a more refined calculation of the integral of thermal conductivity for air in which the effects of the formation of nitric oxide have been included, and the major reactions are considered to occur simultaneously.

SYMBOLS

a	number of mols of reactants (A), also thermal diffusivity, $\frac{k}{C_p\rho}$
A	reactant of a chemical reaction
b	number of mols of products, B
B	product of a chemical reaction
C	specific heat
C_p	specific heat at constant pressure
E_o	energy per mol at zero absolute temperature
k	coefficient of thermal conductivity
$\bar{k}$	average coefficient of thermal conductivity
k^*	coefficient of thermal conductivity for ideal gas with Sutherland correction (see eq. (24))
K_p	chemical equilibrium constant based on partial pressures
N	nitrogen atom

N_2	nitrogen molecule
O	oxygen atom
O_2	oxygen molecule
p	pressure
$p(A_i)$	partial pressure for component A_i
Q	total partition function
Q_p	pQ, partition function for the standard state, 1 atm. pressure
$Q_p(A_i)$	partition function for component A_i
q	heat flow
T	temperature
t	time
x	distance
$X(A_i)$	mols of component A_i per mol of initially undissociated air, or mol concentration
ρ	density
φ	$\int_o^T k\, dT$, heat flux potential
φ^*	$\int_o^T k^* dT$, heat flux potential for ideal gas

Subscripts

i	ith component of gas mixture
o	condition at interface between hot gas and solid wall
1	condition in platinum film

THEORY

Equilibrium Composition of Air

The theoretical and experimental investigation of reference 3 on heat conduction in air covered a range of temperatures and pressures where the dissociation of oxygen and the formation of nitric oxide reach their maximums. However, when the coefficients of thermal conductivity were computed, only the effects of oxygen dissociation were treated because of the order of accuracy being considered. The conductivity calculations of this paper have been refined by the inclusion of the effects of nitric oxide formation, nitrogen dissociation, and all inactive degrees of freedom. This is consistent with the improvement in the experimental procedures and techniques to be described in this paper.

The general approach for the calculation of the equilibrium composition of air is:

1. Establish from the available spectroscopic data, the partition functions of the various constituents of air (N_2, O_2, NO, N, and O) for translational, rotational, vibrational, and electronic excitations.

2. Combine the partition functions to yield the equilibrium constant for each of the three reactions, oxygen dissociation ($O_2 \rightarrow 2O$), nitrogen dissociation ($N_2 \rightarrow 2N$), and nitric oxide formation ($N_2 + O_2 \rightarrow 2NO$).

3. Use the equilibrium constants to establish the set of simultaneous equations from which the equilibrium mol fractions are calculated.

Consequently, the first step is to use the methods of statistical mechanics to formulate the partition functions for the various components in air. The detailed development of the use of partition functions in calculating the thermodynamic and transport properties of air is given in reference 2.

The partition function of a given molecule is defined as

$$Q = \sum_{i=1}^{\infty} g_i e^{-\epsilon_i / kT}$$

which represents the sum of the exponential of every quantum level of energy for all states. The g_i factor, or the degeneracy, accounts for the total number of states which have the same energy level, ϵ_i. The magnitudes of the various energy levels, and the degeneracy of these levels have been accurately established from the spectroscopic data.

In a temperature range of 1000° to 6000° K and a pressure range of 1 to 100 atmospheres, air may be assumed to be made up of N_2, O_2, NO, N, and O. The resulting expressions for the natural logarithms of the partition functions of various species are

$$\ln Q(N_2) = \frac{7}{2} \ln T - 0.42 - \ln \left(1 - e^{\frac{-3390}{T}}\right) - \ln p \tag{1}$$

$$\ln Q(O_2) = \frac{7}{2} \ln T + 0.11 - \ln \left(1 - e^{\frac{-2270}{T}}\right) + \ln \left(3 + 2e^{\frac{-11390}{T}} + e^{\frac{-18990}{T}}\right) - \ln p \tag{2}$$

$$\ln Q(NO) = \frac{7}{2} \ln T + 0.53 - \ln \left(1 - e^{\frac{-2720}{T}}\right) + \ln \left(2 + 2e^{\frac{-174.3}{T}}\right) - \ln p \tag{3}$$

$$\ln Q(N) = \frac{5}{2} \ln T + 0.30 + \ln \left(4 + 10e^{\frac{-27700}{T}} + 6e^{\frac{-41500}{T}}\right) - \ln p \tag{4}$$

$$\ln Q(O) = \frac{5}{2} \ln T + 0.50 + \ln \left(5 + 3e^{\frac{-228}{T}} + e^{\frac{-326}{T}} + 5e^{\frac{-22800}{T}}\right) - \ln p \tag{5}$$

where the spectroscopic constants are obtained from reference 4.

The equilibrium constant, K_p, for each reaction, such as:

$$\Sigma a_i A_i \leftrightharpoons \Sigma b_i B_i \tag{6}$$

is then related to the partition function of the constituents of the reaction through the equation (ref. 5)

$$\ln K_p = -\frac{\Delta E_o}{RT} + \Sigma b_i \ln Q_p(B_i) - \Sigma a_i \ln Q_p(A_i) \tag{7}$$

where

$$\ln Q_p = \ln Q + \ln p \tag{8}$$

and

$$\Delta E_o = \Sigma b_i E_o(B_i) - \Sigma a_i E_o(A_i) \tag{9}$$

that is, the zero point energy of products less the zero point energy of reactants both referred to their standard states. Values of ΔE_o for the various reactions considered here are found in Gilmore's report (ref. 6). Substitution of these values into equation (7) results in the following expressions for the formation of nitric oxide, and the dissociation of oxygen and nitrogen

$$\ln K_p \left(\frac{1}{2} N_2 + \frac{1}{2} O_2 \rightarrow NO \right) = - \frac{10810}{T} + \ln Q_p(NO) - \frac{1}{2} \ln Q_p(N_2) - \frac{1}{2} Q_p(O_2) \tag{10}$$

$$\ln K_p(O_2 \rightarrow 2O) = - \frac{59000}{T} + 2 \ln Q_p(O) - \ln Q_p(O_2) \tag{11}$$

$$\ln K_p(N_2 \rightarrow 2N) = - \frac{113200}{T} + 2 \ln Q_p(N) - \ln Q_p(N_2) \tag{12}$$

According to reference 6, there is also nitric oxide dissociation;

$$NO \rightarrow N + O \tag{13}$$

with a reaction energy between those for oxygen and nitrogen dissociation. As equation (13) does not introduce any element which the other reactions do not include, the number of mols for the different species (N_2, O_2, NO, O, N) can be calculated with any three of the four reactions. Since at high temperatures oxygen and nitrogen dissociations are more important than nitric oxide dissociation, equations (10), (11) and (12) are chosen as the independent reactions for the subsequent analysis, and the reaction of equation (13) is treated as redundant.

The equilibrium constant, K_p, for each reaction, can also be expressed as

$$K_p = \frac{\prod_i [p(B_i)]^{b_i}}{\prod_i [p(A_i)]^{a_i}} \tag{14}$$

through the definition of partial pressure

$$p(A_i) = \frac{X(A_i)}{\Sigma X(A_i) + \Sigma X(B_i)} p \tag{15}$$

where $X(A_i)$ is the number of mols of species A_i per mol of undissociated air. In the remainder of this discussion, $X(A_i)$ will be referred to as the "mol concentration" of species A_i. The sum $\Sigma X(A_i) + \Sigma X(B_i)$ is the total mol concentration of both reactants and products, and p is the total pressure.

In addition, the mol concentration of molecular nitrogen and oxygen can be expressed in terms of the number of mol concentrations of atomic nitrogen and oxygen, and nitric oxide by the following two balance equations:

$$X(O_2) = X_o(O_2) - \frac{1}{2} X(O) - \frac{1}{2} X(NO) \tag{16}$$

$$X(N_2) = X_o(N_2) - \frac{1}{2} X(NO) - \frac{1}{2} X(N) \tag{17}$$

where $X_o(O_2)$ and $X_o(N_2)$ are reference quantities representing the constituents of one mol of air at one atmosphere and 293° K. The numerical values are:

$$X_o(N_2) = 0.78084 \tag{18}$$

$$X_o(O_2) = 0.20946 \tag{19}$$

The remaining 0.0097 mol is composed of inert gases, such as A, He, etc. Substituting equations (15), (16), (17) and the constants of equations (18) and (19) into (14), one obtains the following three equations in terms of the equilibrium constants:

$$[4 - K_p^2(NO)]\, X^2(NO) - K_p^2(NO)\, [X(NO)X(N) + X(N)X(O) + X(NO)X(O) - 1.9806\, X(NO) - 0.41892\, X(N) - 1.56168\, X(O) + 0.65422] = 0 \tag{20}$$

$$\left[4 + \frac{K_p(O)}{p}\right] X^2(O) + \frac{K_p(O)}{p} \left[X(NO)X(N) + X(N)X(O) + X(NO)X(O) + 1.9806\, X(NO) - 0.41892\, X(N) + 1.56168\, X(O) - 0.82971\right] = 0 \tag{21}$$

$$\left[4 + \frac{K_p(N)}{p}\right] X^2(N) + \frac{K_p(N)}{p}\left[X(NO)X(N) + X(N)X(O) + X(NO)X(O)\right.$$

$$\left. + 1.9806\, X(NO) + 0.41892\, X(N) - 1.56168\, X(O) - 3.09306\right] = 0 \qquad (22)$$

The equilibrium mol concentrations of the various species were calculated by solving equations (20), (21), and (22) simultaneously. The computation was done on an IBM 704 computing machine and the results are illustrated in figure 1 as constant-pressure functions of temperature. Values for NO found in this manner were within 1 percent of the results of the detailed calculation performed by Gilmore (ref. 6). The mol concentrations of NO, O, and N are compared in figure 2.

Thermal Conductivity

The thermal conductivity of high-temperature air based on the number of mols of each species is now calculated by taking into account the effects of vibrational and electronic excitation as well as chemical reactions. It is found in the present analysis that the maximum value of mols of NO in air at pressures up to 100 atmospheres is only 11 percent (fig. 1(a)), and it has been observed that the NO molecules have vibrational characteristics similar to those of O_2 and N_2 (ref. 4). Hence, the vibrational and electronic contributions to thermal conductivity in air may be found very closely if it is assumed that there are N_2, O_2, N and O only, and that there is no NO species. Such a procedure is followed by taking directly those values in reference 2 for the vibrational and electronic part of thermal conductivity. The other part of thermal conductivity due to chemical reactions may be obtained by the method of Brokaw and Butler (ref. 7) for simultaneous reactions.[1] The rigorous calculation is rather lengthy and complicated. Fortunately, in the case of simultaneous reactions, such as NO formation and O_2 dissociation, the over-all thermal conductivity can be approximated closely by the sum of thermal conductivities due to each individual reaction (see appendix A).

---

[1]The collision cross section for diffusion is needed for the Brokaw and Butler formula. As previously pointed out by many authors, the collision cross section for diffusion is usually different from that for heat conduction and viscosity. In the case of the NO formation reaction, no accurately determined data exist for the collision cross section of NO with O_2 and N_2. Hence, it is assumed that the collision cross section for diffusion is 0.778 of that for conduction and viscosity, that is, a molecule with a 1/5-power repulsive force (ref. 8, p. 173).

The expression for the total coefficient of thermal conductivity can then be expressed as:

$$k_{total} = k^* + k_{VE} + k_{NO} + k_O + k_N \tag{23}$$

where k^* is defined as the coefficient of thermal conductivity of air which has no vibrational degree of freedom, dissociation, or ionization. Mathematically, it is expressed in reference 2 as:

$$k^* = 1.994 \times 10^{-5} \frac{\sqrt{T}}{1 + \frac{112}{T}} \quad \frac{\text{joules}}{\text{cm-sec-}^\circ\text{K}} \tag{24}$$

The term k_{VE} is defined as the coefficient of thermal conductivity due to electronic and vibrational excitation of all molecules, k_O, the contribution due to oxygen dissociation, k_N, the contribution due to nitrogen dissociation, and k_{NO}, the contribution due to nitric oxide formation. The component thermal conductivities are shown in figure 3 in terms of the ratio of the coefficient k to the reference quantity k^*.

Comparisons of the partial thermal conductivities for the various degrees of freedom are shown in figure 4. The effect of molecular vibration becomes appreciable at temperatures above 500° K, that of NO formation above 1500° K, and that of O_2 dissociation above 2000° K. It may also be observed that the slope of the curve is greater if the activation energy involved is greater. Thus, the curve for vibrational and electronic excitation has the smallest slope whereas the curve for O_2 dissociation has the largest slope. The thermal conductivity for the various degrees of freedom becomes pressure dependent toward higher temperatures, as seen from the separation of the curves for the various pressures. The separation of the curves for the combination of vibrational and electronic degrees of freedom is due to the pressure dependence of the formation of atoms which become electronically excited at higher temperatures. The separation of the curves for NO formation and O_2 dissociation are reflections of changes in the equilibrium mol concentrations of species involved in the reactions. In general, the pressure dependence of the thermal conductivity of air can be attributed mainly to oxygen dissociation. For the range of temperatures investigated the total coefficient of thermal conductivity is shown in figure 3(e).

Heat Conduction Between Two Semi-Infinite Media

The computed value of thermal conductivity can now be related to the specific case of time-dependent one-dimensional heat conduction through a semi-infinite gas medium at constant pressure with uniform initial conditions. The partial differential equation governing this process is

$$C_p\rho \frac{\partial T}{\partial t} - \frac{\partial}{\partial x}\left(k \frac{\partial T}{\partial x}\right) = 0 \tag{25}$$

This equation can be solved by specifying the quantity

$$\varphi = \int_0^T k_{total}\, dT = \bar{k}T \tag{26}$$

as the dependent variable instead of T itself (ref. 3). This quantity will be called the heat-flux potential. Substitution of equation (26) into equation (25) results in the following partial differential equation with φ as the dependent variable:

$$\frac{\partial \varphi}{\partial t} - a \frac{\partial^2 \varphi}{\partial x^2} = 0 \tag{27}$$

where the thermal diffusivity, $a = k/C_p\rho$.

The theoretical components of φ are obtained by integrating the theoretical values of each component of k in equation (23) according to equation (26). The total heat-flux potential is expressed in dimensionless form by dividing each component by φ^*. This quantity is defined as the heat-flux potential for ideal air and is given by:

$$\varphi^* = \int_0^T k^*\, dT \tag{28}$$

where k^* is given by equation (24). Numerical values for this integral are shown in figure 5.

The total heat-flux potential, expressed in dimensionless form, φ/φ^*, is then equal to

$$\frac{\varphi}{\varphi^*} = 1.0 + \left(\frac{\varphi}{\varphi^*}\right)_{VE} + \left(\frac{\varphi}{\varphi^*}\right)_{NO} + \left(\frac{\varphi}{\varphi^*}\right)_{O} + \left(\frac{\varphi}{\varphi^*}\right)_{N} \tag{29}$$

where the 1.0 denotes the idealized air value, $(\varphi/\varphi^*)_{VE}$ the contributions from vibration and electronic excitations, $(\varphi/\varphi^*)_{NO}$ the contribution of nitric oxide formation, $(\varphi/\varphi^*)_{O}$ the contribution of oxygen dissociation, and $(\varphi/\varphi^*)_{N}$ the contribution of nitrogen dissociation. Variations of these components with temperature are shown in figure 6.

The heat-flux potential as a function of temperature can also be obtained by combining the solution of the partial differential equation (27)

A 4 0 1

with experimental measurements of certain boundary conditions. The equation can be solved if two boundary conditions are available: (1) the interface temperature at the wall which is evaluated by the use of a thin film gage (a detailed description of gage construction and performance is given in the experiment section), and (2) the initial state of the high-temperature air in the region behind the reflected shock, which is a known function of the incident shock-wave speed. The measurement of these two quantities permits the calculation of the gradient of thermal conductivity which exists in the gas at the interface, where the temperature rise is relatively small. Once the value of the gradient at the interface is specified, one can integrate the differential equation (27) to obtain the value of the integral of thermal conductivity for the high-temperature air in the region behind the reflected shock. The qualitative form of the solution for the limiting value of φ as a function of $(\partial\varphi/\partial x)_o$ is shown in sketch (a). The numerical value of φ is determined from these graphical solutions using the measured value for $(\partial\varphi/\partial x)_o$. Details of this approach can be found in reference 3. These solutions will be compared with the theory in a subsequent section of this report.

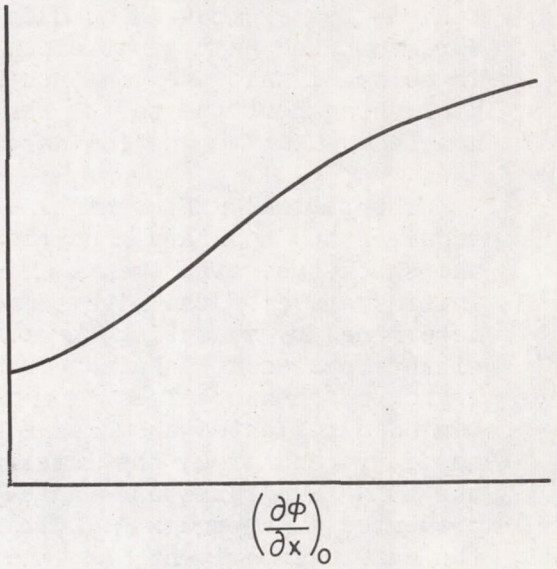

Sketch (a)

EXPERIMENT

Only a brief description of the shock-tube apparatus is presented in this paper since a detailed description is available in reference 3. This section will be more concerned with improvements in experimental procedures, and improvements in the design and manufacture of the film gages used to measure temperature at the wall of the shock tube.

The shock tube used to generate high-temperature air for the experiments consists of a reservoir chamber initially filled with high-pressure helium and a test tube initially filled with air at relatively low pressures (usually less than one atmosphere). The two sections are separated by a diaphragm. Upon rupture of the diaphragm, a strong shock forms near the diaphragm, travels down the tube at high speed, accelerating and compressing the air after it, and then on reaching the end of the tube is reflected back toward the reservoir. The actual test phase begins at the instant the incident shock wave is reflected from the end of the shock tube. At this instant the air sample has been brought to rest by the reflection so that heat diffusion in air which is in a state of high temperature and pressure can be studied in the absence of strong heat convection effects. Relaxation effects do not seem to be large since the relaxation time is of the order of 10 microseconds as compared with the minimum testing time of 200 microseconds. Temperature detection is accomplished by a thin film resistance gage mounted flush with the wall at the

end cap of the shock tube. A schematic diagram for the test section is shown in sketch (b). During the test period, the reflected shock wave

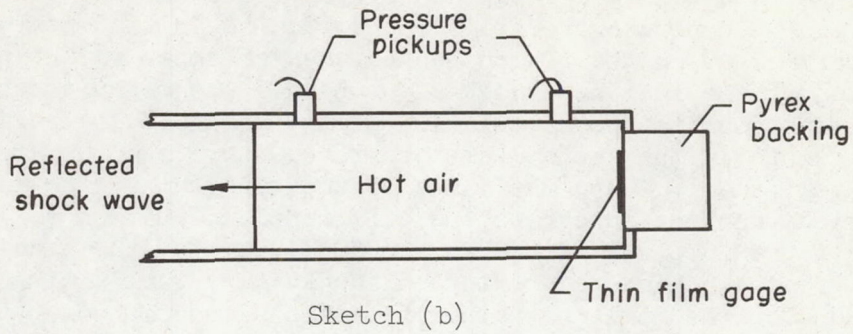

Sketch (b)

travels faster than the cooling influence of the heat-diffusion process. Moreover, the heat penetration into the pyrex backing of the film gage is so small that the 1/4-inch thick pyrex is practically an infinite heat sink throughout the test. Hence, there occurs the one-dimensional, nonsteady heat conduction described in the Theory section.

The partial differential equation (eq. (27)) governing this process requires two boundary conditions for its solution. Both are found from the shock-tube experiment. The first boundary condition required is the initial state of the high-temperature air. The shock-wave speed is determined by measuring the time for the shock to traverse two pressure pickups spaced at a known distance. The state of the air in the test region is then obtained from reference 9 which presents the state variables behind a reflected shock as a function of the shock speed. The second boundary condition, the interface temperature at the wall, is measured by the thin film-resistance gage. (A discussion of this thin film gage is presented in appendix B.) This measurement is the most critical one of the entire experiment, as it is believed that the scatter of the data in reference 3 can be attributed mainly to the erratic behavior of the film gages used in that experiment. The improved gage used for this experiment is of the same type, a resistance thermometer with a microsecond response time. The measuring circuit is a Wheatstone bridge with the film gage as one of its arms. The signal is recorded on an oscilloscope.

The construction of the improved gage is somewhat different from that described in reference 3. The gage which yielded the most satisfactory results for the present series of tests is shown in figure 7(a) in four stages of manufacture. These stages are:

1. A rectangular prism with grooved sides is formed from pyrex to serve as a base for the gage.

2. The grooves are coated with three layers of Hanovia Platinum-Bright solution no. 5. The gage is baked after each coating at 1100° F for 20 minutes, followed by a cooling period of 8 hours or more.

3. The film gage is formed by painting a platinum strip 1/16 inch wide across the face of the prism from one groove to the other to form a continuous path. The gage is baked in the same manner as in step 2.

4. Lead wires are soft soldered to the coated grooves. Precautions are taken against overheating during the soldering process so as not to destroy the resistance characteristics of the film. The purity of the soft solder is also checked as it was found that impurities increased the terminal resistance and decreased the gage sensitivity.

Figure 7(b) shows the completed gage mounted in the holder with a resin cement. The final step is to coat the face of the gage with a 1000 Å layer of electrically inert silicone monoxide. The purpose of this coating is to protect the film from free electron or ion interference from the partially ionized air. Initial experiences with uncoated film gages showed spurious, fast pulse signals of large amplitude at higher temperatures where ionization occurs. Similar experiences were reported in reference 10 and were attributed to charge pickup from the ionized gas. It is assumed that the coated gages, which produce outputs free of such spurious pulses, indicate the correct temperature except for the time lag effect produced by the silicone monoxide coating.

The experimental procedure was also changed from that used in the experiments of reference 3. The following steps also tended to eliminate some of the scatter in the data:

1. The original film gages were calibrated in a water bath calorimeter (see ref. 3). However, this type of calibration is very time consuming and does not simulate the fast step impulse of temperature obtained under actual test conditions. A capacitor discharge calibration was tried, similar to that reported in reference 11, but this also did not simulate the condition that heat flux varies as the square root of time. For a true simulation, the shock tube itself was used for calibration of the film gage at gas temperatures below 1000° K (i.e., low shock strength). At these test conditions the interface temperature jumped approximately 10° K above atmospheric temperature after the reflection of the shock wave. At these temperatures where the thermal conductivity has been established, an equivalent constant for temperature resistivity was found by equating the experimental conductivity to the known values. This constant was then used to analyze the data for higher temperature tests where the interface temperature rise varied from 20° K to 60° K.

2. Prior to the test, both the reservoir chamber and test tube were evacuated to eliminate any contamination. In addition, the test tube underwent a purge cycle three times.

3. During testing, a high-frequency vibration produced by the rupture of the diaphragm, was evidenced by a fluctuating signal from the film gage. Further examination revealed that the vibration was being transmitted to spring-type connections at the open ends of the lead wire. A solder connection at this location eliminated the spurious signal.

Some typical temperature records registered by these gages are shown in figure 8. The appropriate test conditions for each record are indicated on the figure.

DISCUSSION OF RESULTS

The theoretical values of φ/φ^* are obtained from figure 6 for the experimentally determined temperatures and pressures. The variation of pressure with increasing temperature (i.e., increasing shock strength) for this series of experiments can also be seen in figure 6(b). The over-all potential is obtained theoretically by evaluating the components φ/φ^* for the various modes of excitation and the various reactions, then algebraically adding the components. At temperatures ranging from 600° K to 2000° K, the increase in the over-all heat-flux potential above the ideal-gas value of 1.0, can be attributed to the vibrational and electronic modes of excitation. The formation of nitric oxide starts at 1000° K, although its effect on φ/φ^* does not become noticeable until a temperature of 2000° K is reached. At this point, oxygen dissociation is initiated, and by the time a temperature of 3000° K is reached, the φ/φ^* contribution due to oxygen dissociation is of the same magnitude as those for the vibrational and electronic modes and for nitric oxide formation. Above 4000° K the theoretical value of the dimensionless heat-flux potential levels out slightly and then increases again. This variation indicates that the nitric oxide formation and oxygen dissociation are nearly complete, and that nitrogen dissociation is beginning.

The theoretical value of φ/φ^* is compared in figure 9 with the values of φ/φ^* obtained by using experimental boundary values to solve the one-dimensional heat-flow equation (eq. (23)). The experimental and theoretical φ/φ^* agree very well in a temperature range from 1000° to 4600° K. Since the coefficient of thermal conductivity, k/k^*, can be derived from the slope of the temperature versus heat-flux curve (fig. 9), the comparison of experimental and theoretical heat-flux potentials is then a direct indication of the accuracy with which the coefficient of thermal conductivity has been predicted. However, the uncertainty in the determination of a derivative from any experimental data is relatively large. In this light, the close correlation between experimental and theoretical estimates of the heat flux can be interpreted as a necessary but not sufficient criterion that the coefficient of thermal conductivity has been accurately predicted. The close correlation does indicate that the predicted coefficients of thermal conductivity may have suitable accuracy for many engineering needs.

CONCLUDING REMARKS

Computed values of the integral of the coefficient of thermal conductivity for high-temperature air were checked by Hansen, et al., in NASA TR R-27, by comparing the theoretical values of the integral of thermal conductivity (heat-flux potential) with the experimental values of the integral obtained from shock-tube measurements. However, the correlation between theory and experiment was uncertain, mainly because of the large scatter in the experimental data. A much closer correlation has been obtained in this paper by using a more refined calculation of thermal conductivity, and by using improved experimental techniques.

The theoretical integral of thermal conductivity is obtained by algebraically adding the integrals for the excitations of the various degrees of freedom for the components of air, and to the chemical reactions between these components. This calculation must include the excitation of the vibrational and electronic modes, and the formation of nitric oxide, as well as the dissociation of oxygen considered in reference 3. The inclusion of these additional effects is necessary because they determine almost entirely the deviation of thermal conductivity from the perfect gas value for temperatures up to 3000° K.

The most critical measurement of the entire experiment is the measurement of the interface temperature at the wall of the shock tube by a thin film resistance gage. Consistent and accurate temperature data are obtained if the following steps are taken: (1) positive binding between the painted platinum film strip and the pyrex backing; (2) protection of the film and terminal connections from extraneous electrical pickup and damage from the high-temperature air, and (3) calibration of the resistance gage during actual shock-tube experiments at low temperatures where the variation of the coefficient of thermal conductivity with temperature has been definitely established.

As a result of these factors, a much closer correlation is shown between the experimental and theoretical integrals of thermal conductivity. This close correlation is a necessary but not sufficient criterion that the coefficient of thermal conductivity has been accurately predicted. The close correlation does indicate that the predicted coefficients of thermal conductivity may have suitable accuracy for many engineering needs, up to the limits of the test (4600° K).

Ames Research Center
National Aeronautics and Space Administration
Moffett Field, Calif., Oct. 31, 1960

APPENDIX A

INDEPENDENCE OF THERMAL CONDUCTIVITY

In a pure dissociating gas, such as O_2 or N_2, the thermal conduction at high temperatures can be ascribed to two simultaneous processes: (1) conduction by molecular and atomic collisions, (2) conduction in the form of transported chemical enthalpy of dissociated molecules due to concentration gradients (i.e., chemical diffusion). For a gas mixture such as air, where both of these species are dissociating and NO is forming and dissociating, the basic mechanism for thermal conduction is the same. Collision occurs between particles of all the components in the mixture (i.e., O_2, NO, N, etc.). However, the transport rate of chemical enthalpy of dissociated molecules for each reaction is affected by the presence of the other reactions, though the other reactions may be quiescent at a given state condition. This effect is included by Butler and Brokaw (ref. 7) in the following expression for the thermal conductivity due to chemical diffusion.

$$k_r = -\frac{1}{RT^2}\frac{\begin{vmatrix} 0 & \Delta H_1 & \Delta H_2 \\ \Delta H_1 & A_{11} & A_{12} \\ \Delta H_2 & A_{21} & A_{22} \end{vmatrix}}{\begin{vmatrix} A_{11} & A_{12} \\ A_{21} & A_{22} \end{vmatrix}}$$

for the case where two reactions are simultaneously occurring. The ΔH's are the heats of reaction for each reaction alone, A_{ii} is a measure of the reaction rate of the ith reaction alone, and A_{ij} is a measure of the change in the reaction rate of the ith reactions due to the presence of the jth reaction. The A's are expressed in reference 7 as functions of the number of mols and the collision cross sections for the various combinations of reacting particles.

Rewriting the expression for k_r, and setting

$$|A| = \begin{vmatrix} A_{11} & A_{12} \\ A_{21} & A_{22} \end{vmatrix}$$

one has,

$$k_r = -\frac{1}{RT^2}\left[\frac{\Delta H_1 \Delta H_2}{|A|}(A_{12} + A_{21}) - \frac{\Delta H_1{}^2 A_{22}}{|A|} - \frac{\Delta H_2{}^2 A_{11}}{|A|}\right]$$

Now, if $A_{12} = A_{21} < A_{11}$ or A_{22}, and $A_{12}A_{21} \ll A_{11}A_{22}$,

then,

$$k_r \cong \frac{1}{RT^2}\frac{\Delta H_1^2}{A_{11}} + \frac{1}{RT^2}\frac{\Delta H_2^2}{A_{22}}$$

The first term on the right side of the above equation is the thermal conductivity due to the first reaction alone as indicated by ΔH_1, and, similarly, the second term is due to the second reaction with ΔH_2 only. Hence, for the approximations stated above, the over-all thermal conductivity, k_r, is equal to the sum of thermal conductivities that result from first and second reactions, respectively.

The magnitudes of A_{ij}'s for the simultaneous reactions will now be examined. The atomic collision cross sections for diffusion were obtained from reference 2, and the molecular collision cross sections for diffusion were obtained by correcting the collision cross sections for conduction in reference 2 by a factor of 0.778 as suggested in reference 8 for a molecule with a 1/5-power repulsive force. In the case of three simultaneous reactions, such as NO formation, O_2 dissociation, and N_2 dissociation, the N_2 dissociation has only a small effect in the region of temperature considered in this report; and between NO formation and O_2 dissociation, the magnitudes of the A_{ij} terms are:

$$\left.\begin{aligned} A_{12} = A_{21} &= 2.681\times10^5 \ \frac{\text{cm-sec}}{\text{mol}} \\ A_{11} &= 29.91\times10^5 \ \frac{\text{cm-sec}}{\text{mol}} \\ A_{22} &= 22.44\times10^5 \ \frac{\text{cm-sec}}{\text{mol}} \\ \frac{A_{12}}{A_{11}} &\cong \frac{1}{10}, \quad \frac{A_{12}}{A_{22}} \cong \frac{1}{10} \end{aligned}\right\} \text{for } T = 3348^\circ \text{ K}, \ p = 10.74 \text{ atm}$$

$$\left.\begin{aligned} A_{12} = A_{21} &= 2.389\times10^5 \ \frac{\text{cm-sec}}{\text{mol}} \\ A_{11} &= 66.51\times10^5 \ \frac{\text{cm-sec}}{\text{mol}} \\ A_{22} &= 1.029\times10^8 \ \frac{\text{cm-sec}}{\text{mol}} \\ \frac{A_{12}}{A_{11}} &\cong \frac{1}{30}, \quad \frac{A_{12}}{A_{22}} \cong \frac{1}{500} \end{aligned}\right\} \text{for } T = 2647^\circ \text{ K}, \ p = 19.69 \text{ atm}$$

These calculations show that it is reasonable to assume that the over-all thermal conductivity due to NO formation, O_2 dissociation, and N_2 dissociation is equal to the sum of the contributions from each reaction.

In a private communication, Dr. Brokaw stated that where the off-diagonals (i.e., A_{12}) are as much as 20 to 50 percent of the diagonal terms (i.e., A_{11}, A_{22}), the error in thermal conductivity introduced by neglecting the off-diagonals is only 5 percent at worst.

APPENDIX B

THEORY OF THIN FILM THERMOMETRY

The theory of thermometry for a thin film gage may be outlined as follows: Consider a one-dimensional nonsteady heat conduction (sketch c).

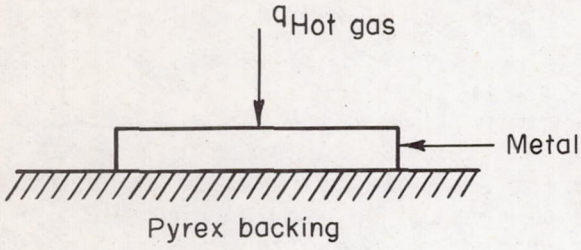

Sketch (c)

Heat is being transferred from the hot gas through a layer of metal to glass. It is physically true that the temperature and heat flow on the gas side of metal are different from those on the glass side. The difference is caused by the fact that the metal needs heat to adjust its thermal level with the gas and the glass on two sides and that it takes a finite time for the heat-conduction process to be complete. However, both temperature and the heat-flow differences can be reduced to a negligibly small amount for a thin gage so that the heat-conduction process will be maintained practically the same as if there were no metal film in between.

It is further reasoned from reference 3 that for a gas instantly heated in a shock tube, the interface temperature between the metal and gas will remain constant and the heat flow at that interface will be inversely proportional to the square root of time. Mersman, Berggren, and Boetler arrived at essentially the same conclusion in dealing with heat conduction between two semi-infinite solids (ref. 12). If only the heat conduction inside the metal is considered and a perfect contact is assumed, the temperature and heat flow at any point inside the metal may be obtained from the equations in reference 12. Using temperature, T_o, and heat flow at the interface, Q_o, as boundary conditions, one obtains the following expressions:

$$\frac{T(x,t)}{T_o} = 1 - \left[\left(1 - \frac{T_1}{T_o}\right) \operatorname{erf}\left(-\frac{x}{2\sqrt{a_1 t}}\right)\right]$$

$$\frac{Q(x,t)}{Q_o} = e^{-\frac{x^2}{4a_1 t}}$$

where

$$Q_o = \frac{T_o - T_1}{\sqrt{\pi a_1 t}} K_1$$

where T_1 is initial temperature of metal and a_1 is the thermal diffusivity of the metal, which is taken to be a constant. For $x = 2000$ Å, $t = 1$ μsec, and a platinum film,

$$\frac{T(x,t)}{T_o} = 1 - 0.0027 = 0.9973$$

$$\frac{Q(x,t)}{Q_o} = 1 - 2.4 \times 10^{-4} = 0.99986$$

The results are applicable for the case where there is no glass backing, but a semi-infinite extension of metal. Since glass has smaller thermal conductivity, the deviations for temperature and heat flow will certainly be much less than indicated above. Hence, one can be assured that in using the thin film gage of only 2000 Å thickness, one obtains essentially the surface temperature and heat flow for the backing material.

REFERENCES

1. Hirschfelder, J. O., Curtiss, C. F., and Bird, R. B.: Molecular Theory of Gases and Liquids. John Wiley and Sons, Inc., New York, 1954.

2. Hansen, C. Frederick: Approximations for the Thermodynamic and Transport Properties of High-Temperature Air. NASA TR R-50, 1959.

3. Hansen, C. Frederick, Early, Richard A., Alzofon, Frederick E., and Witteborn, Fred C.: Theoretical and Experimental Investigation of Heat Conduction in Air, Including Effects of Oxygen Dissociation. NASA TR R-27, 1959.

4. Herzberg, G.: Molecular Spectra and Molecular Structure. I. Spectra of Diatomic Molecules. D. Van Nostrand Co., 1950.

5. Glasstone, Samuel: Theoretical Chemistry. D. Van Nostrand Co., 1944.

6. Gilmore, F. R.: Equilibrium Composition and Thermodynamic Properties of Air to 24000° K. Rand Report, RM-1543, 1955.

7. Butler, James N., and Brokaw, Richard S.: Thermal Conductivity of Gas Mixtures in Chemical Equilibrium. Jour. of Chem. Phys., vol. 26, no. 6, June 1957, pp. 1636 to 1643.

8. Chapman, S., and Cowling, T. G.: The Mathematical Theory of Non-Uniform Gases. Second ed., Cambridge Univ. Press., 1952.

9. Hansen, C. Frederick, and Heims, Steve P.: A Review of the Thermodynamic, Transport and Chemical Reaction Rate Properties of High Temperature Air. NACA TN 4359, July 1958.

10. Jahn, Robert R., and Weimer, David: On the Performance of Thin-Film Gages in High-Temperature Shock Tube Flows. Jour. Appl. Phys., vol. 29, no. 4, Apr. 1958, pp. 741-742.

11. Rabinowicz, J., Jessey, M. E., and Bartsch, C. A.: Resistance Thermometer For Heat Transfer Measurement in a Shock Tube. Calif. Inst. of Tech., Guggenheim Aero. Lab., Memo. 33, July 2, 1956.

12. Mersman, W. A., Berggren, W. P., and Boelter, L. M. K.: The Conduction of Heat in Composite Infinite Solids. Univ. of California Press, 1942.

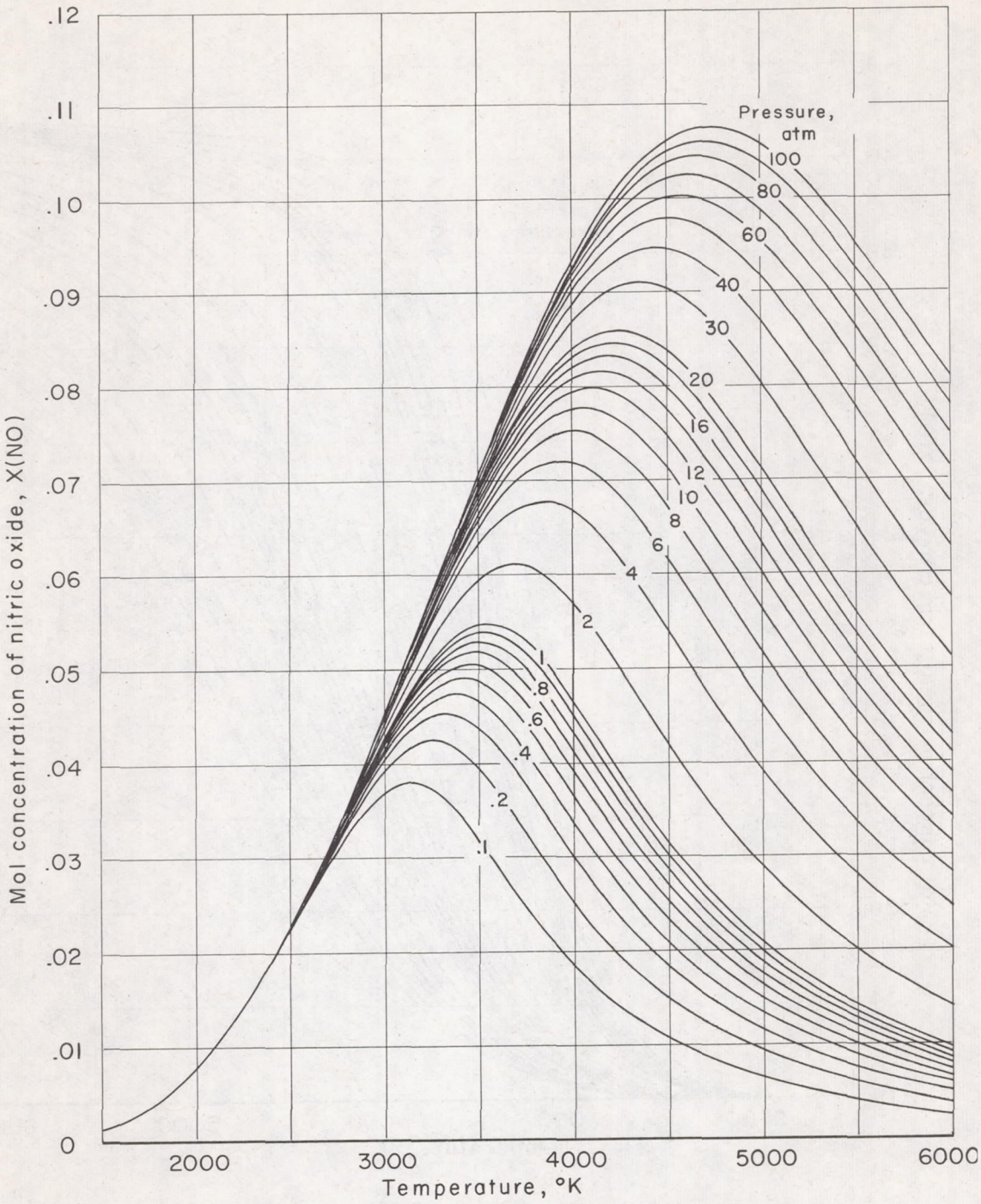

(a) Nitric oxide.

Figure 1.- Equilibrium mol concentration of air components.

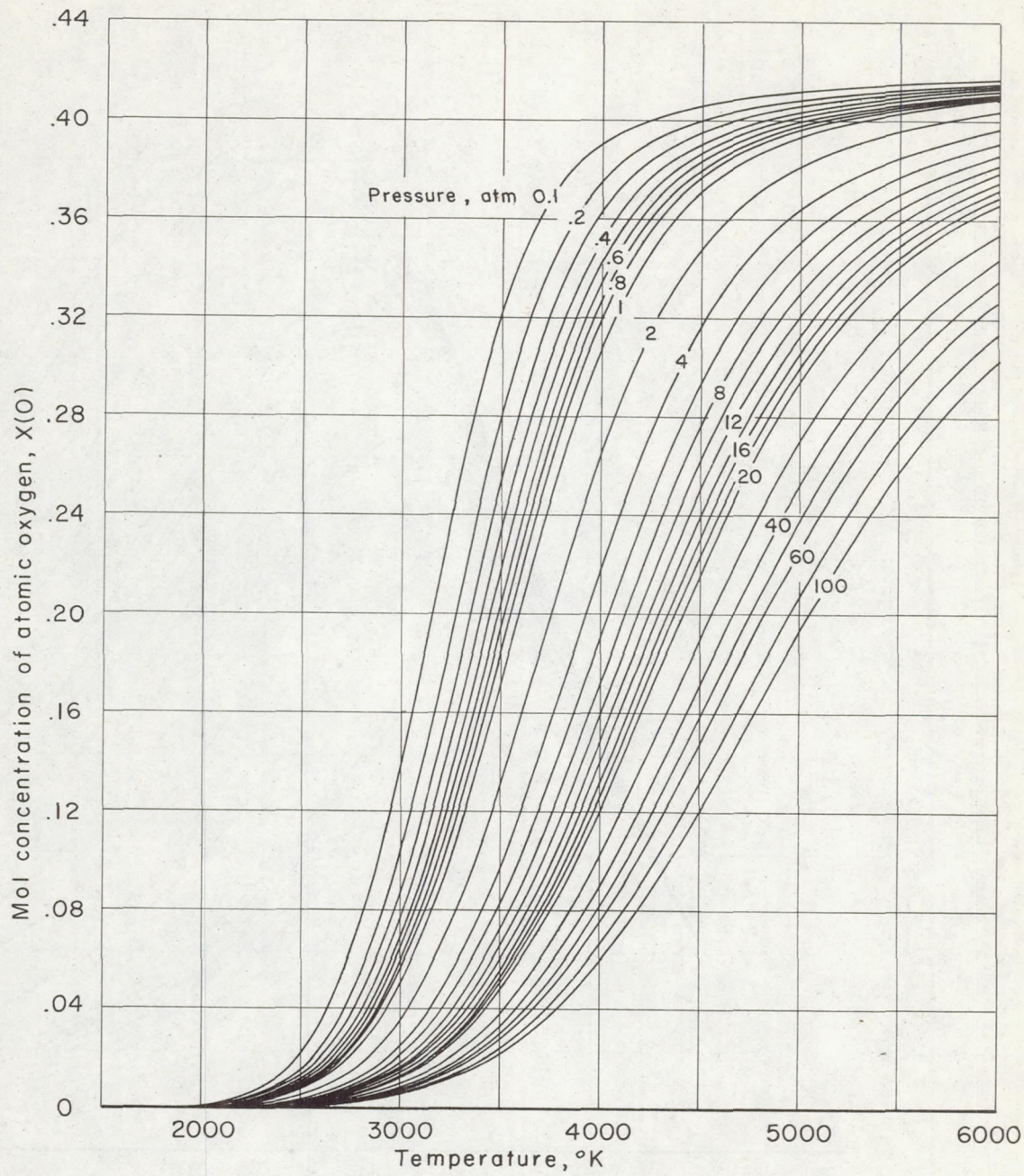

(b) Atomic oxygen.

Figure 1.- Continued.

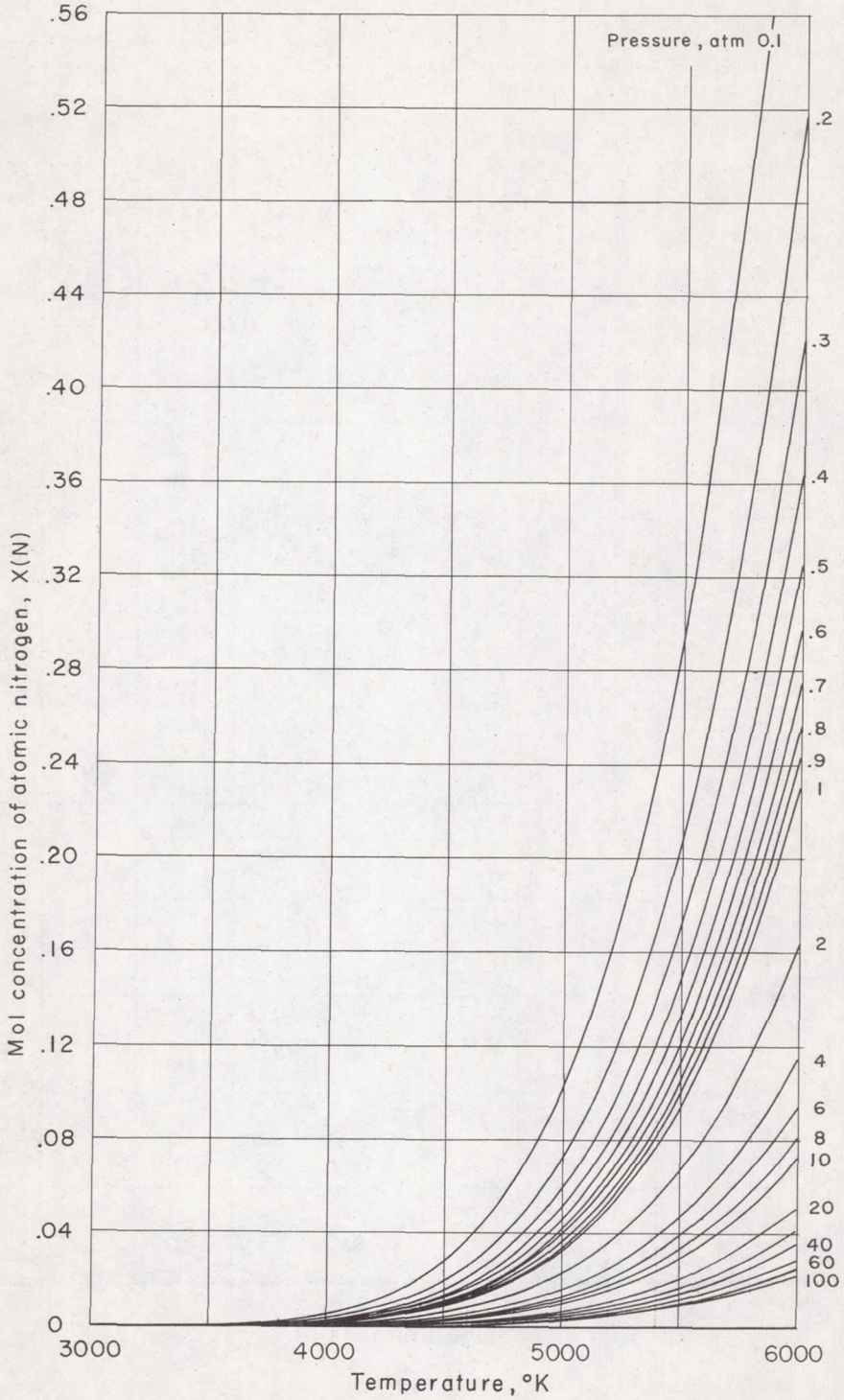

(c) Atomic nitrogen.

Figure 1.- Concluded.

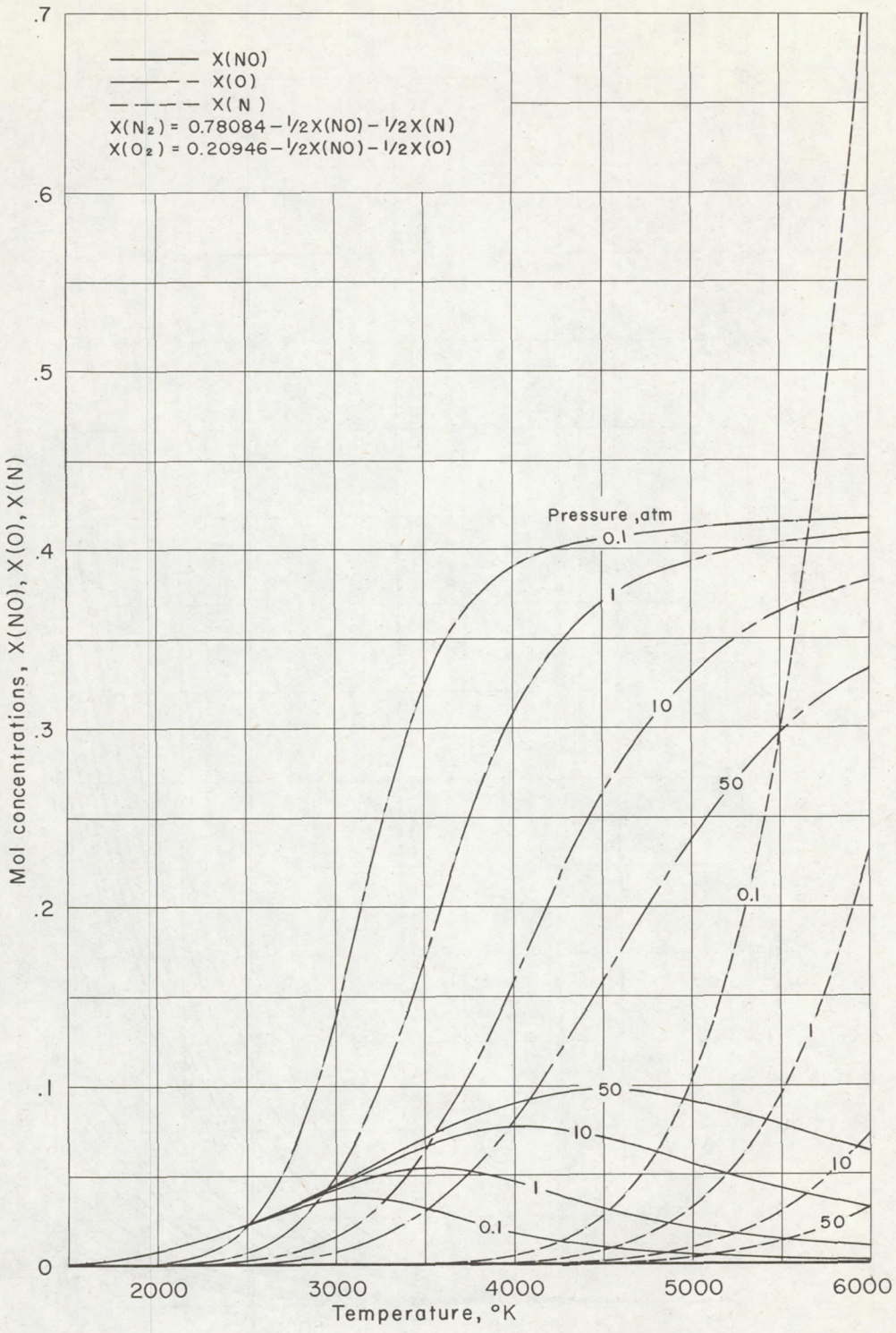

Figure 2.- Component mols of air in equilibrium.

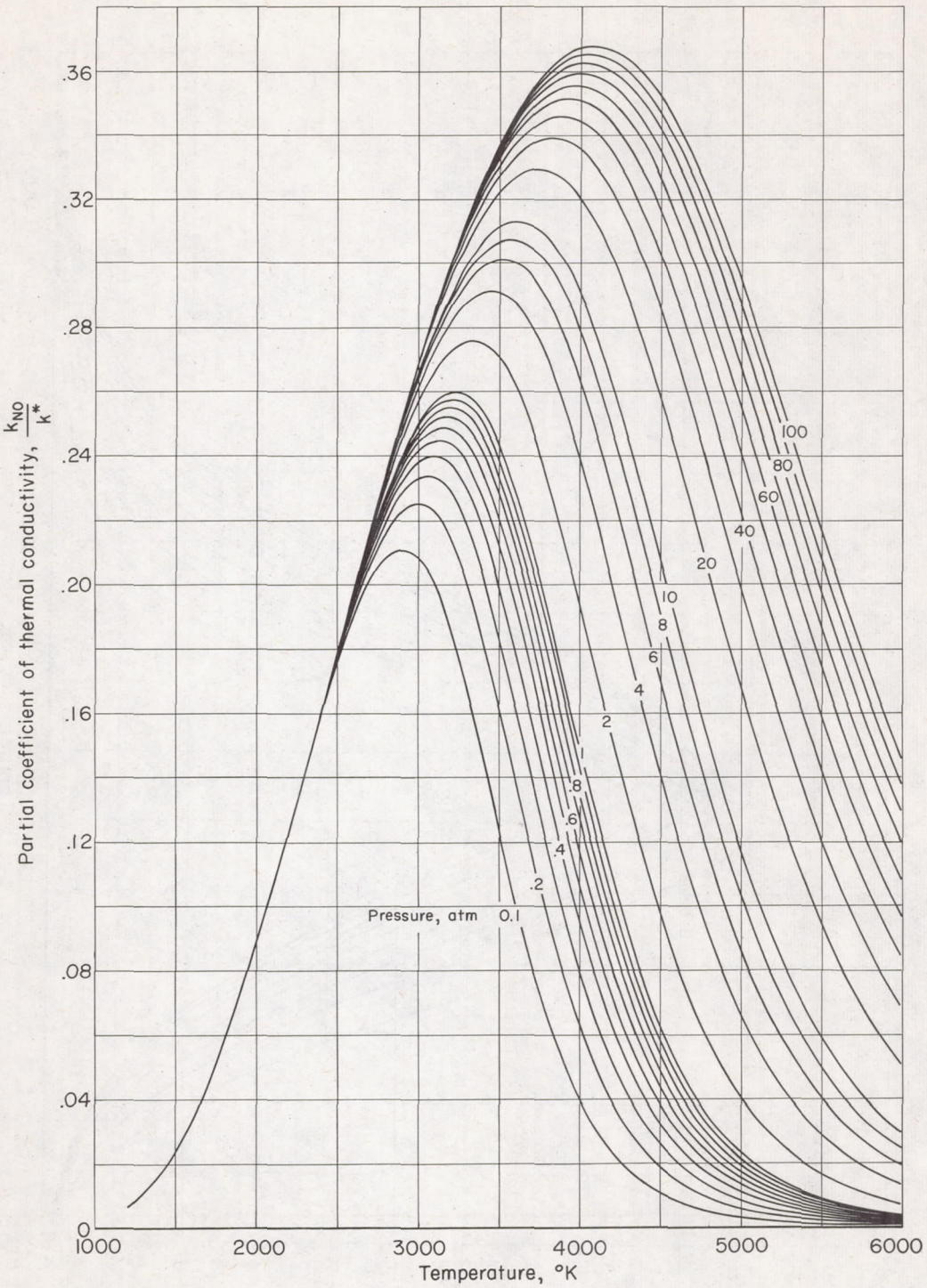

(a) Nitric oxide formation.

Figure 3.- Coefficients of thermal conductivity.

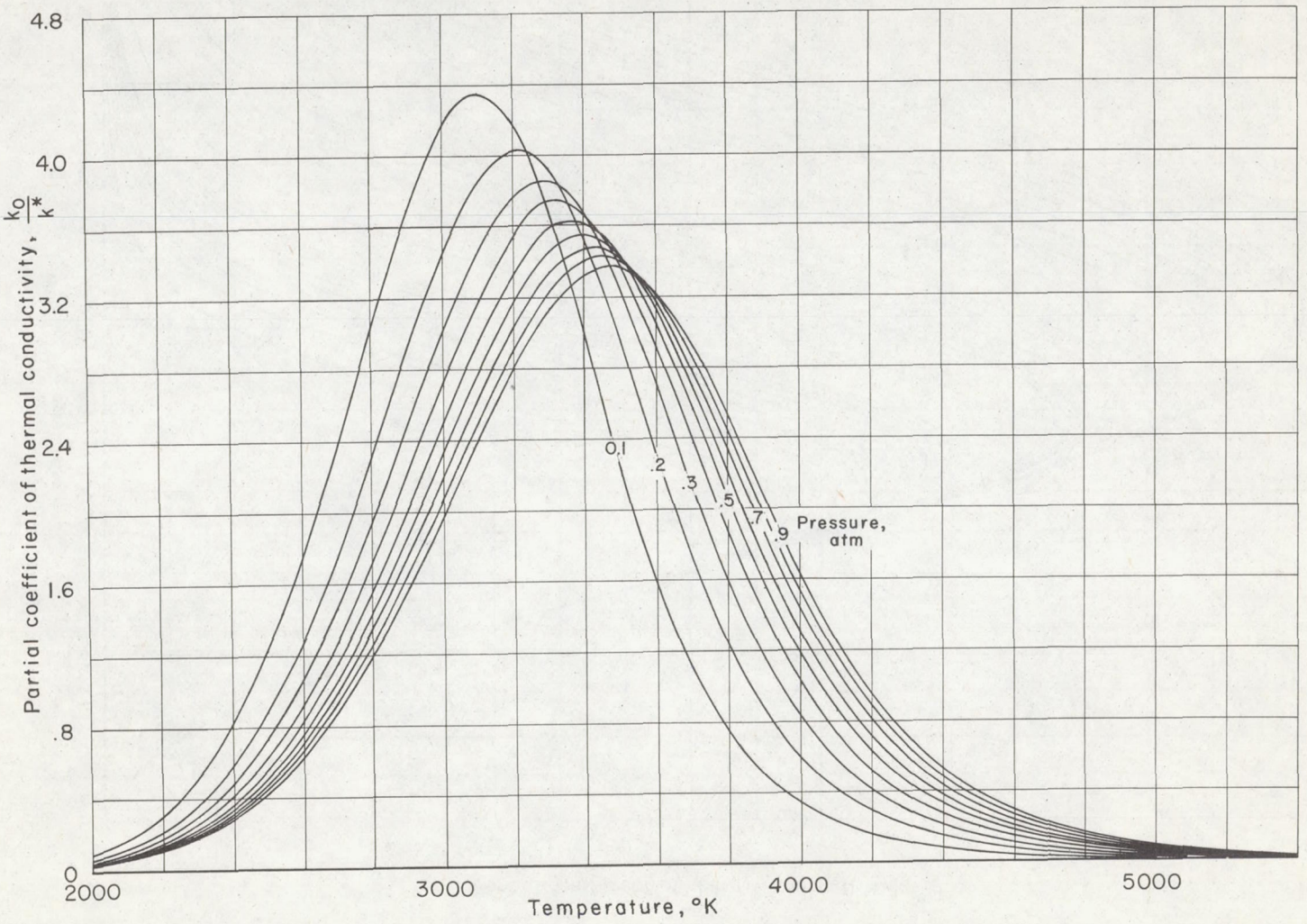

(b) Oxygen dissociation 0.1 to 0.9 atm. pressure.

Figure 3.- Continued.

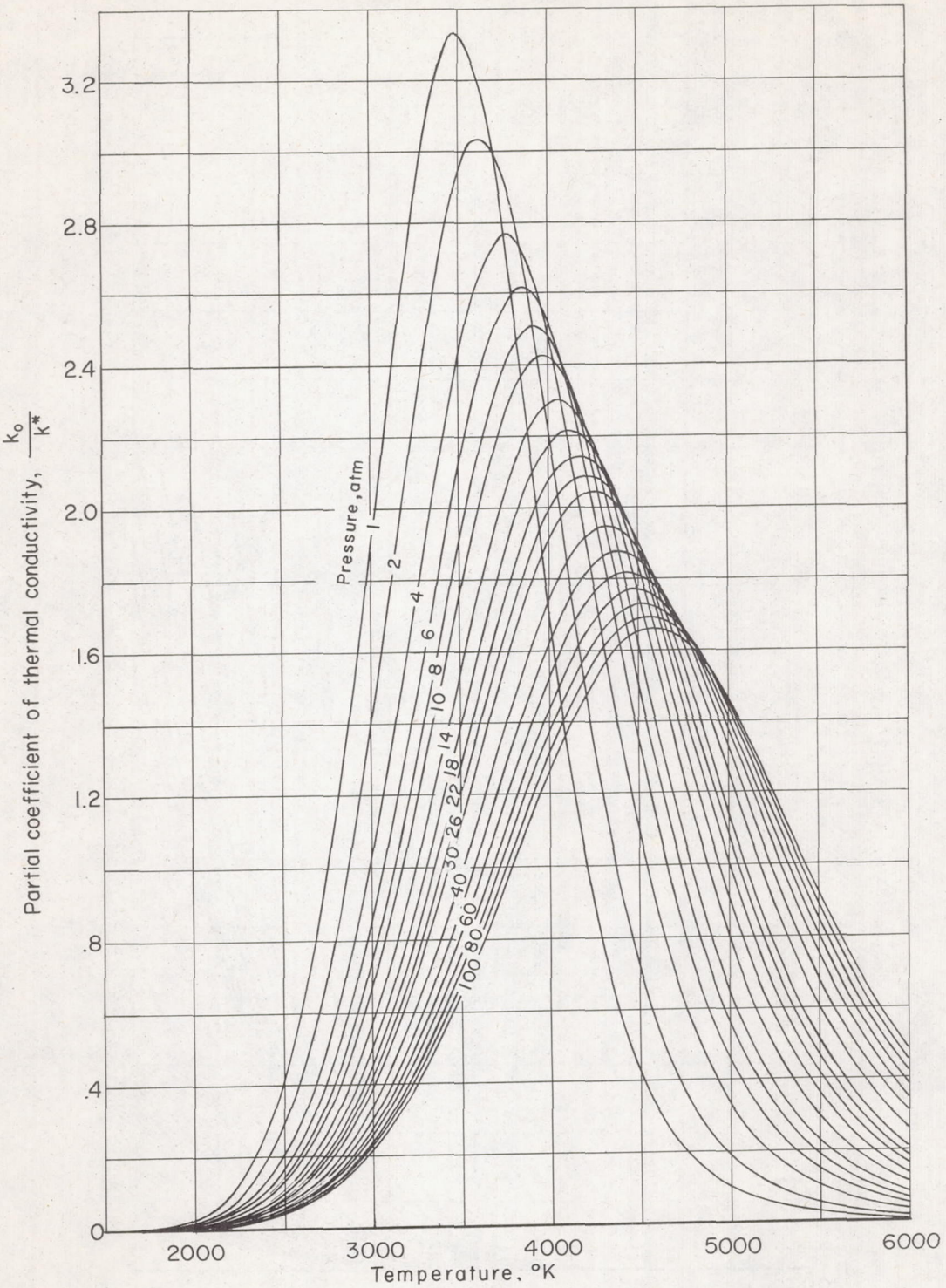

(c) Oxygen dissociation, 1 to 100 atm. pressure.

Figure 3.- Continued.

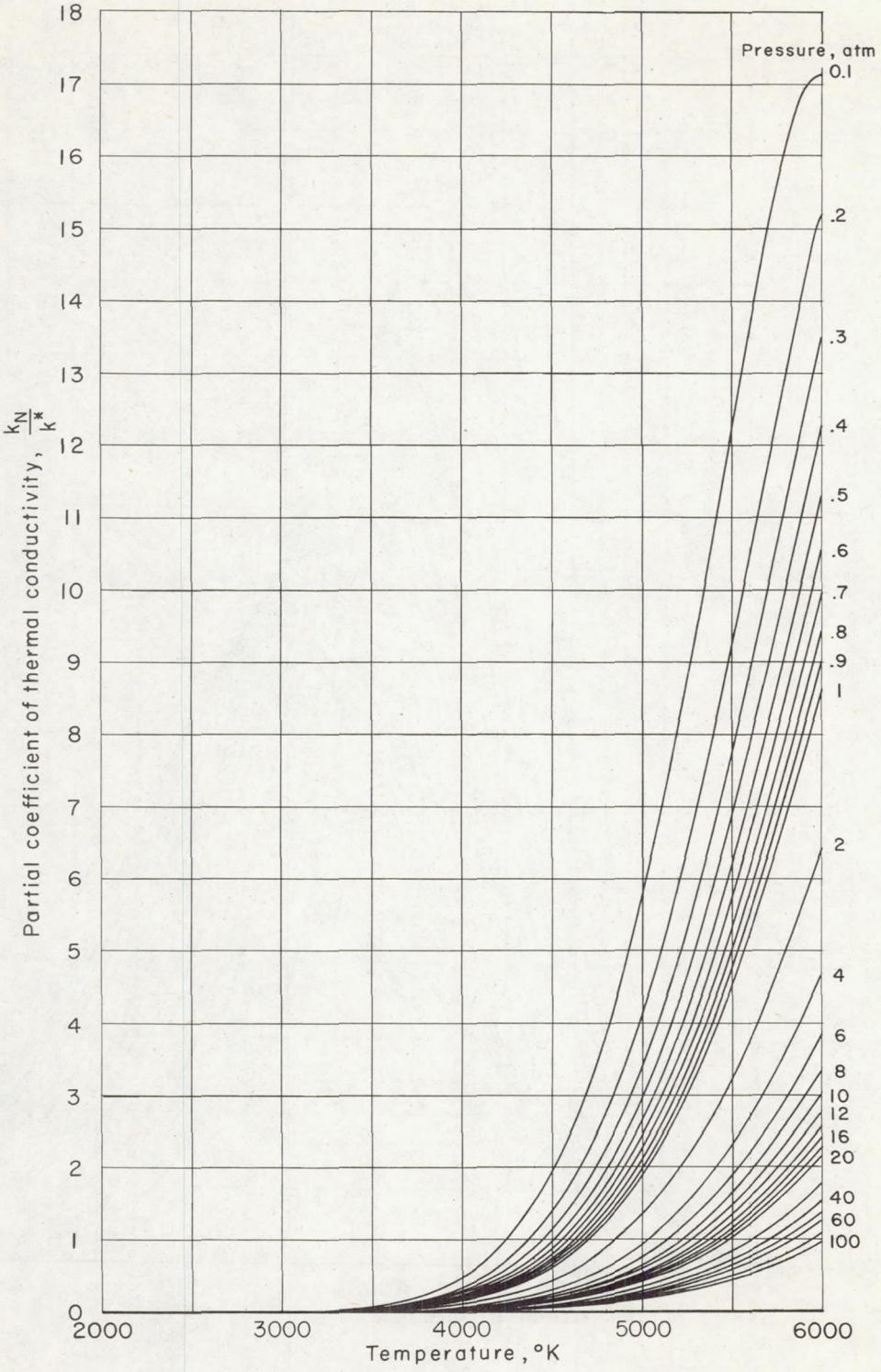

(d) Nitrogen dissociation.

Figure 3.- Continued.

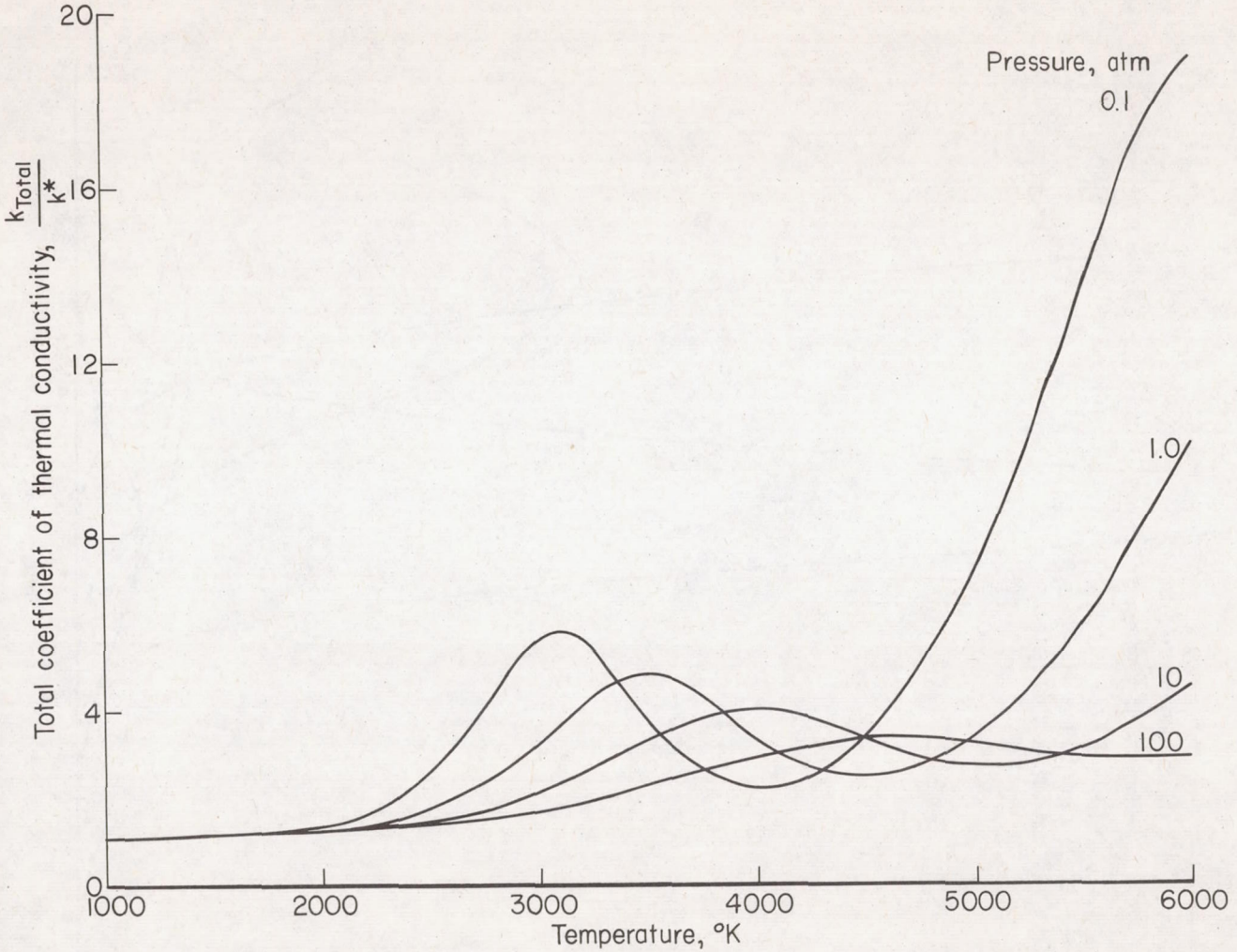

(e) Total coefficient of thermal conductivity.

Figure 3.- Concluded.

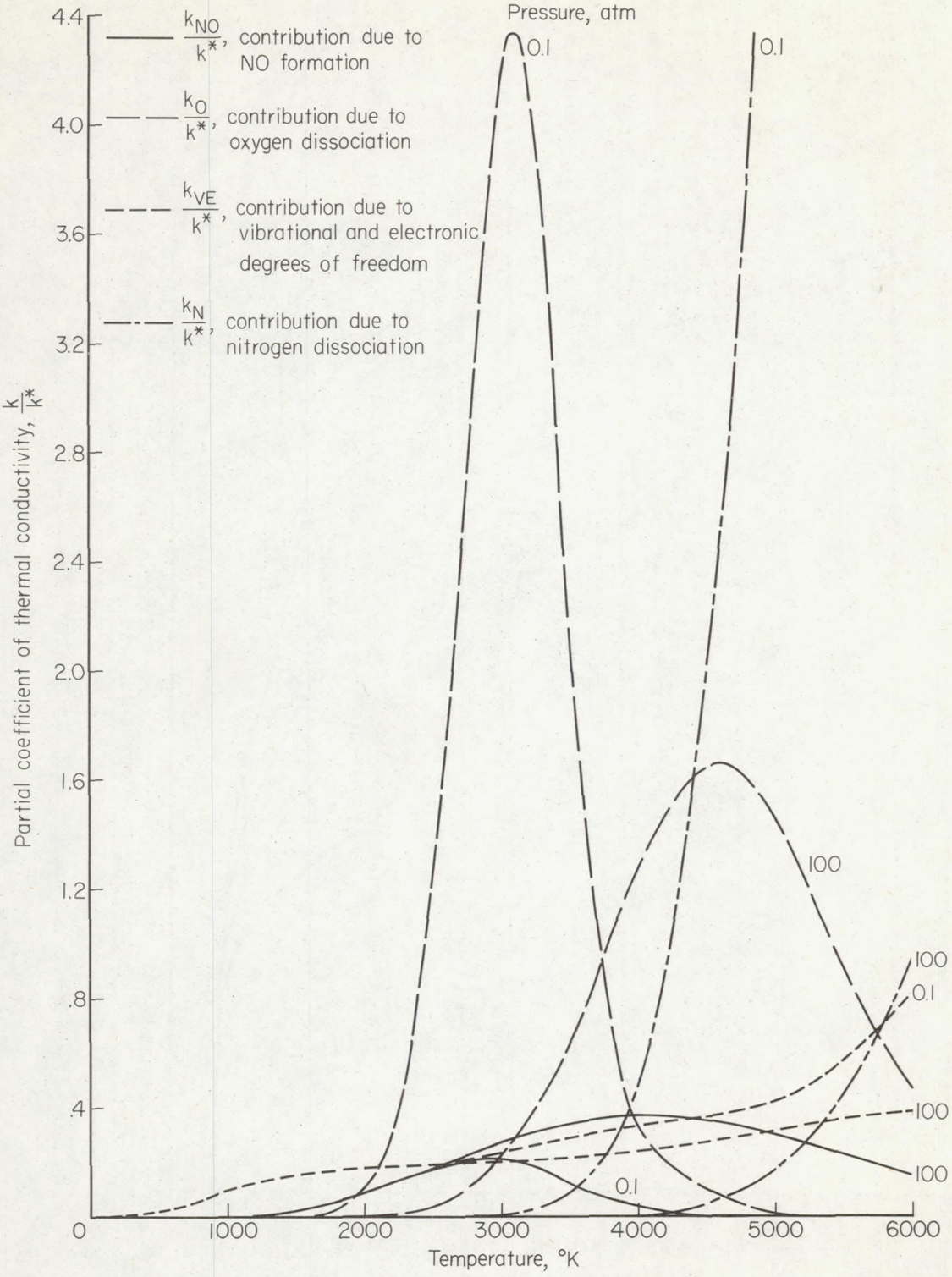

Figure 4.- Comparison of the partial coefficients of thermal conductivity.

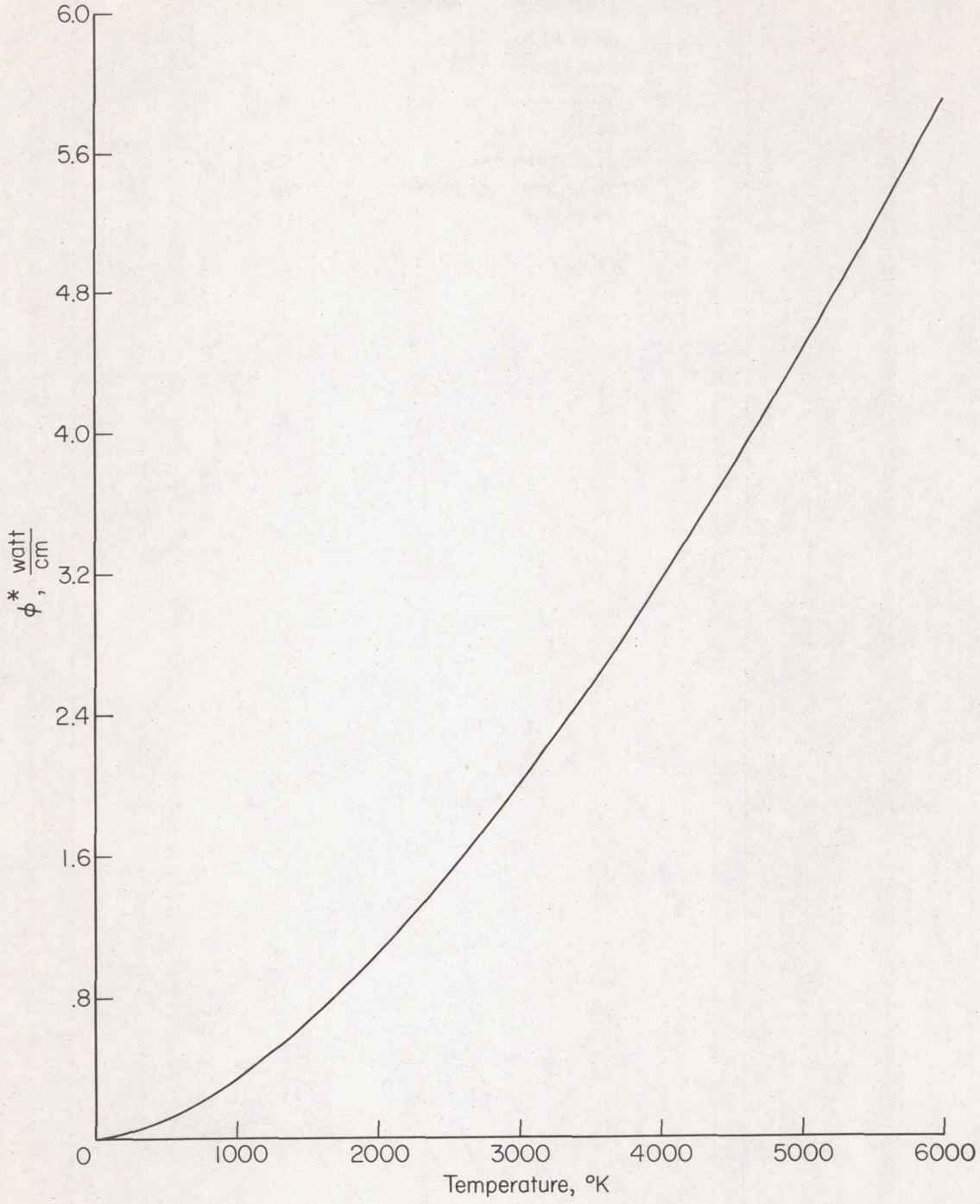

Figure 5.- Integral of reference thermal conductivity, φ^*.

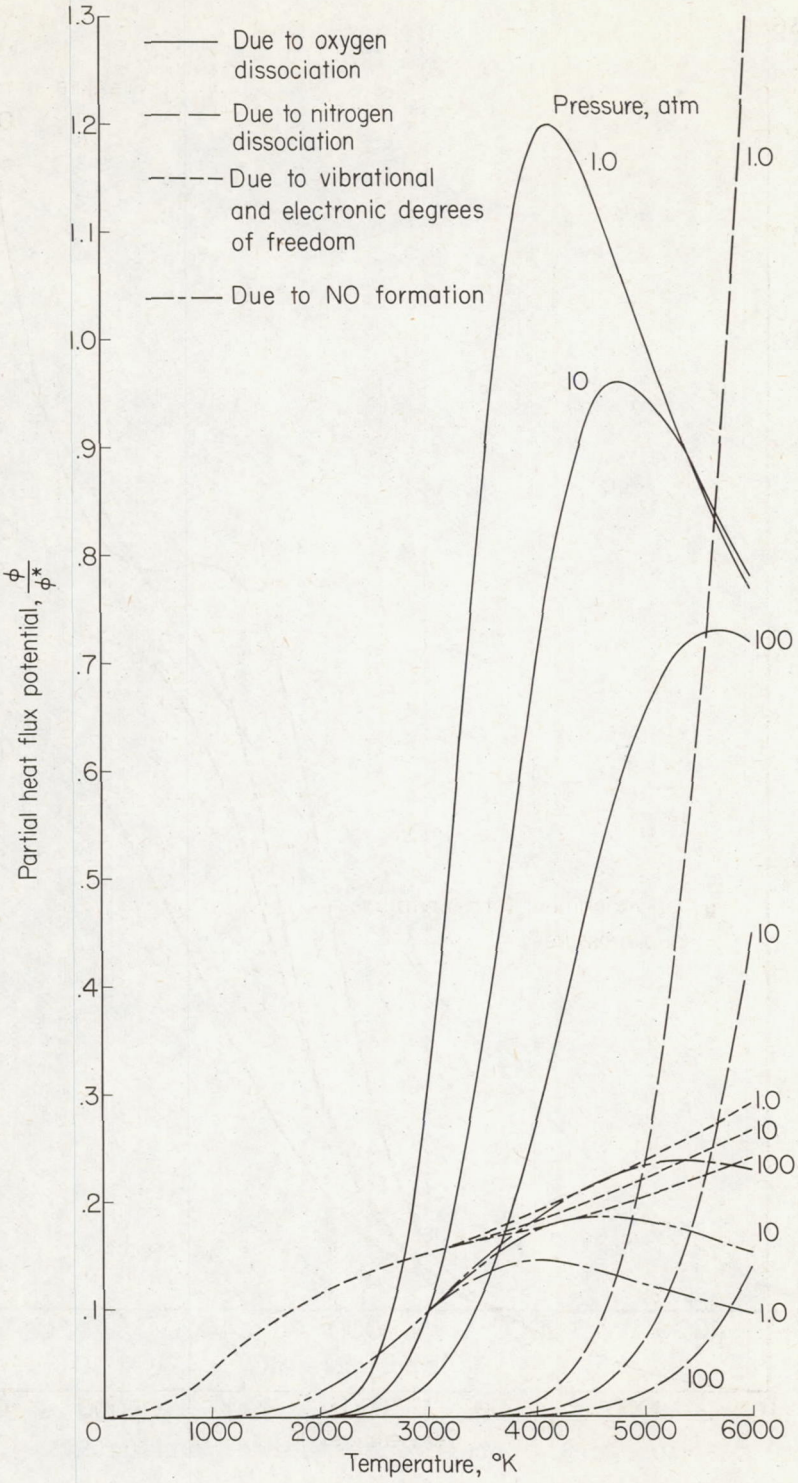

(a) Partial heat flux potentials.

Figure 6.- Heat flux potentials.

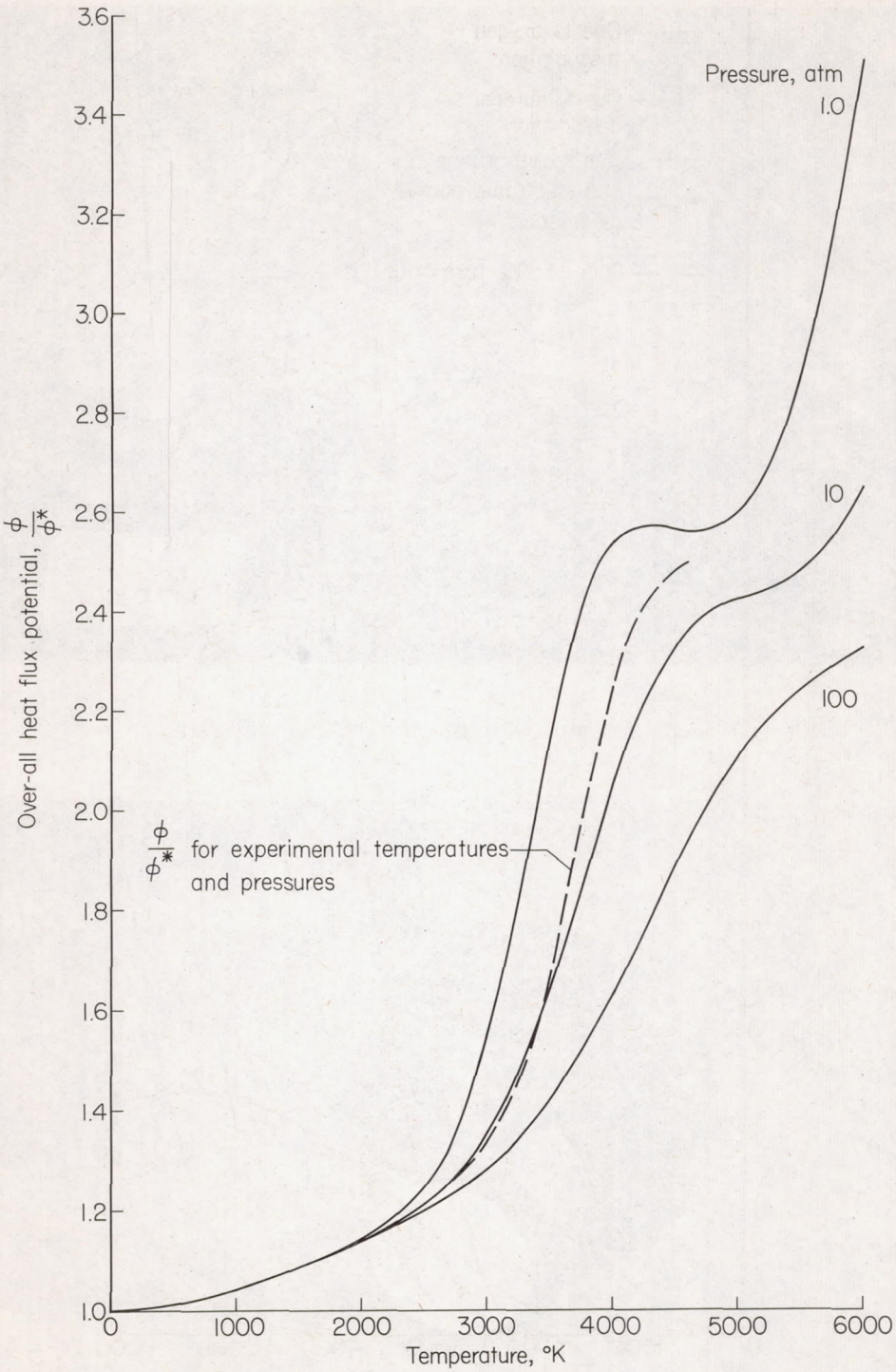

(b) Total heat flux potentials.

Figure 6.- Concluded.

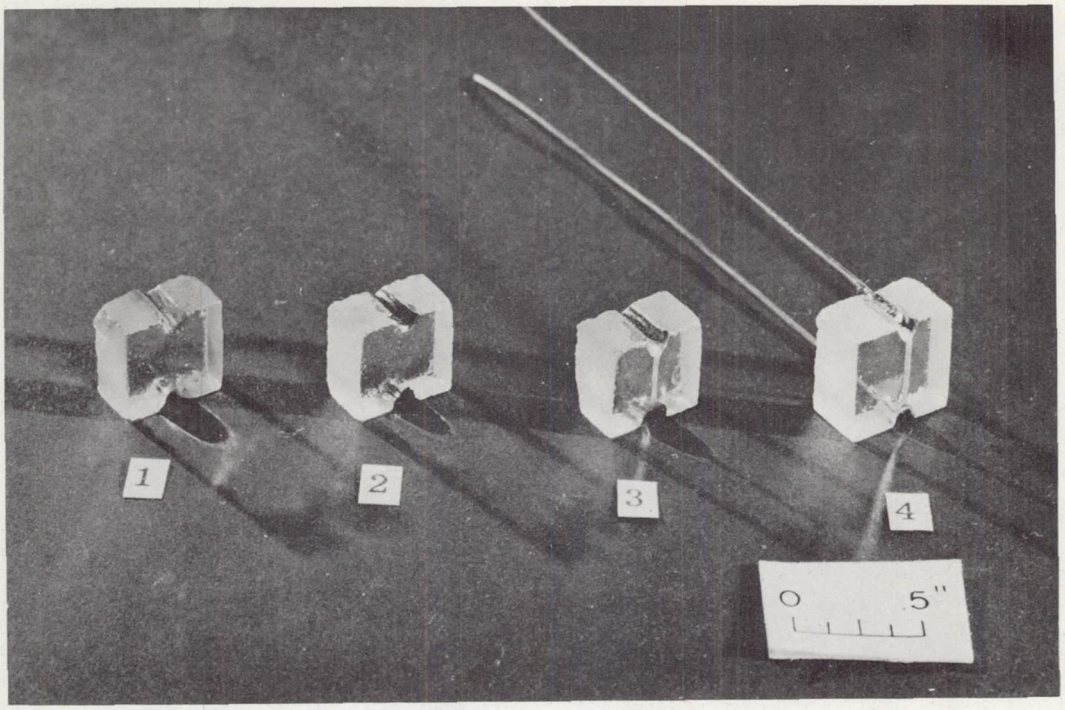

A-26366

(a) Gage in various stages of manufacture.

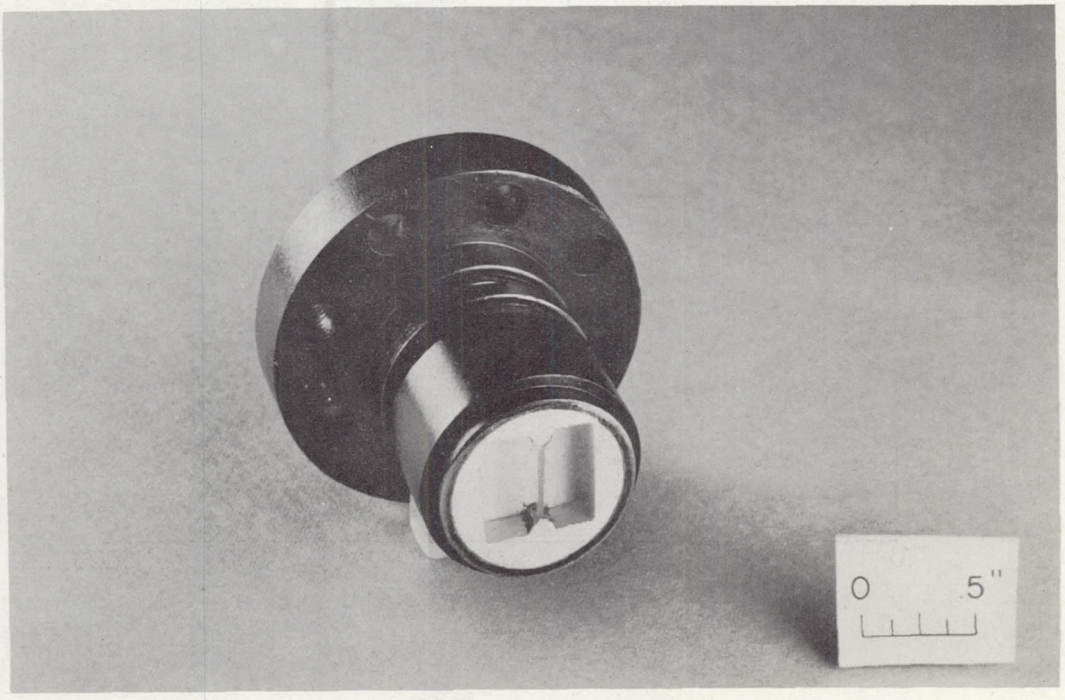

A-26367

(b) Gage mounted in holder.

Figure 7.- Photographs of thin film gage.

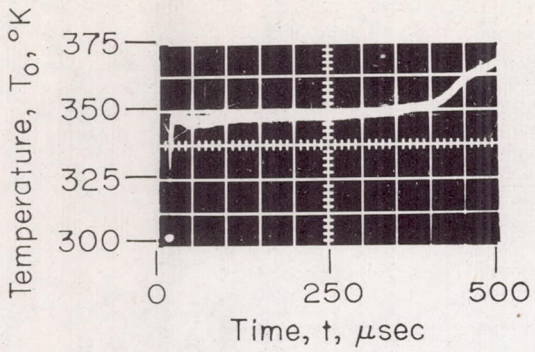

(a) $M_1 = 5.88$, $p_3 = 12.96$ atm, $T_3 = 3294^\circ$ K

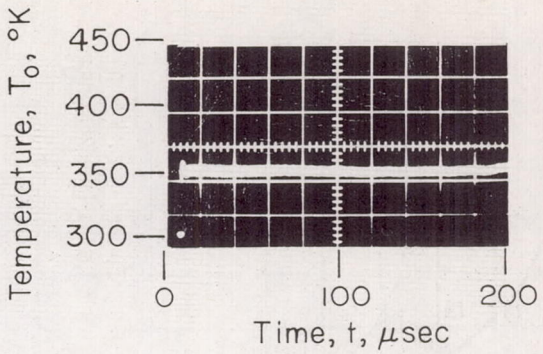

(b) $M_1 = 7.02$, $p_3 = 7.72$ atm, $T_3 = 3956^\circ$ K

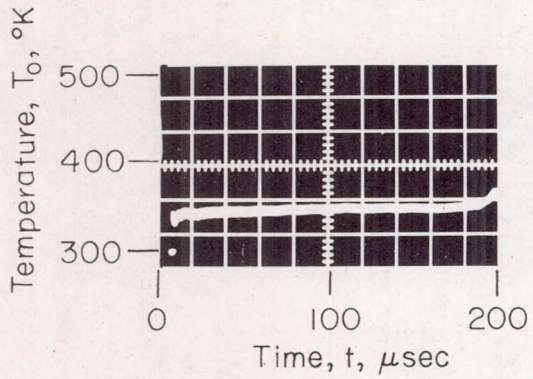

(c) $M_1 = 8.185$, $p_3 = 3.1$ atm, $T_3 = 4468^\circ$ K

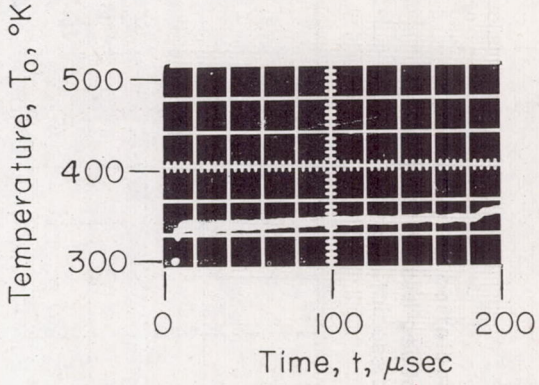

(d) $M_1 = 8.525$, $p_3 = 1.76$ atm, $T_3 = 4630^\circ$ K

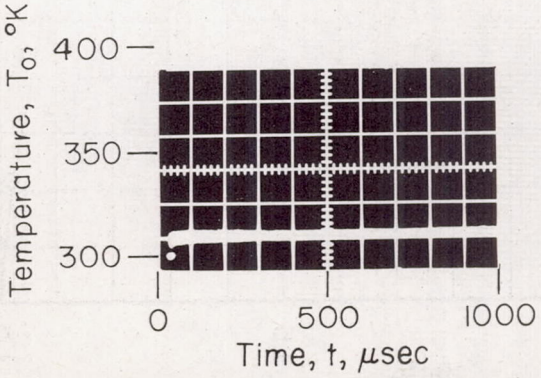

(e) $M_1 = 2.079$, $p_3 = 23.1$ atm, $T_3 = 686.5^\circ$ K

Figure 8.- Records of temperature at the surface of a pyrex slab.

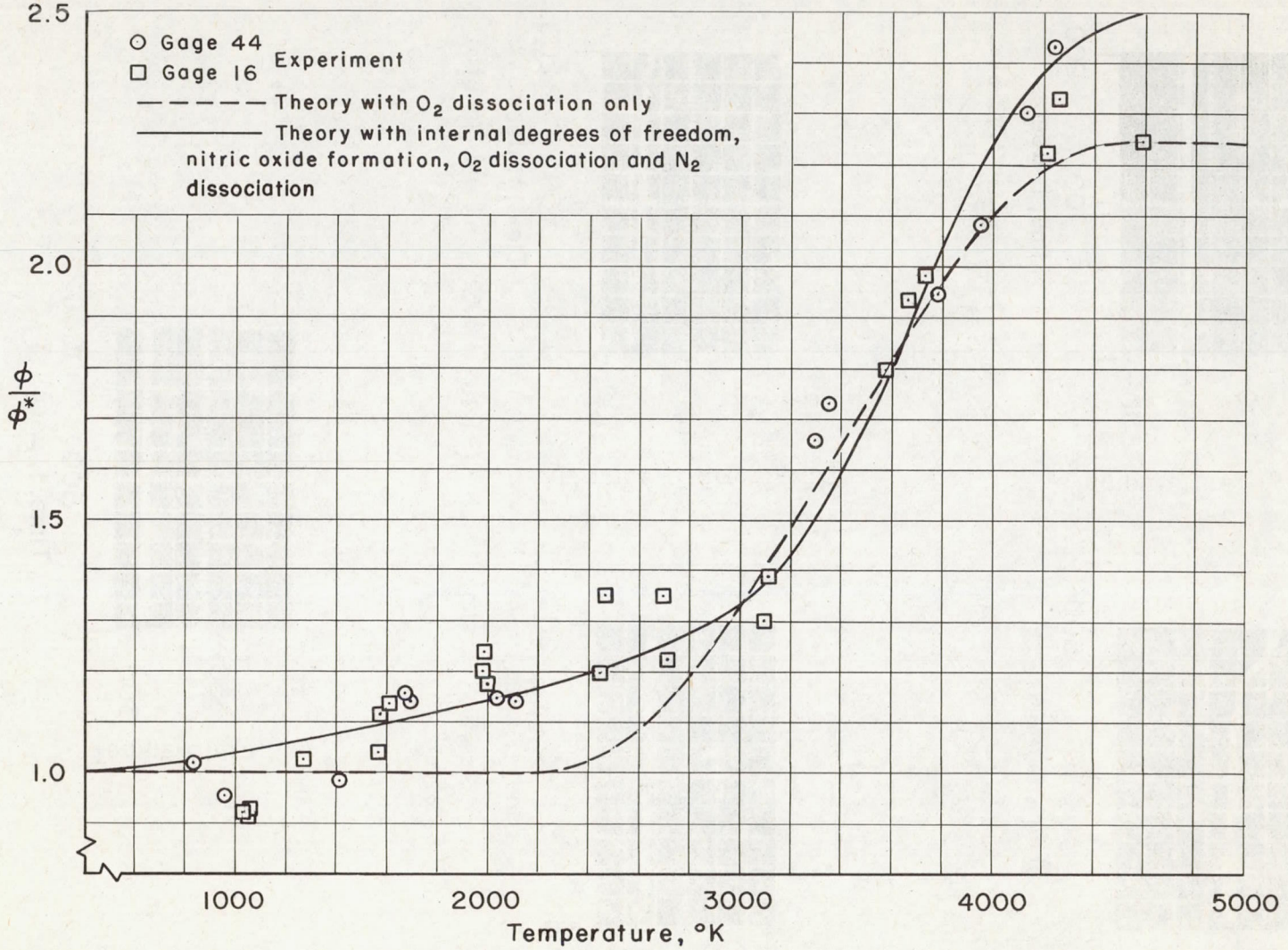

Figure 9.- Comparison of experimental and theoretical integrals of thermal conductivity.